Computational and Structural Biotechnology Journal 20 (2022) 882–890

COMPUTATIONAL AND STRUCTURAL BIOTECHNOLOGY JOURNAL

journal homepage: www.elsevier.com/locate/csbj

Identification of novel SARS-CoV-2 RNA dependent RNA polymerase (RdRp) inhibitors: From *in silico* screening to experimentally validated inhibitory activity

Tanaporn Uengwetwanit [a,*], Nopporn Chutiwitoonchai [a], Kanin Wichapong [b], Nitsara Karoonuthaisiri [a,c]

[a] National Center for Genetic Engineering and Biotechnology (BIOTEC), National Science and Technology Development Agency, Pathum Thani 12120, Thailand
[b] Department of Biochemistry, Cardiovascular Research Institute Maastricht (CARIM), Maastricht University, 6200 MD Maastricht, the Netherlands
[c] Institute for Global Food Security, Queen's University, Belfast, Biological Sciences Building, 19 Chlorine Gardens, Belfast BT9 5DL, United Kingdom

ARTICLE INFO

Article history:
Received 8 December 2021
Received in revised form 1 February 2022
Accepted 1 February 2022
Available online 04 February 2022

Keywords:
SARS-CoV-2
Coronavirus
Inhibitor
Molecular docking
Virtual screening
Drug discovery

ABSTRACT

The emergence of severe acute respiratory syndrome coronavirus 2 (SARS-CoV-2) in 2019 has posed a serious threat to global health and the economy for over two years, prompting the need for development of antiviral inhibitors. Due to its vital role in viral replication, RNA-dependent RNA polymerase (RdRp) is a promising therapeutic target. Herein, we analyzed amino acid sequence conservation of RdRp across coronaviruses. The conserved amino acids at the catalytic binding site served as the ligand-contacting residues for *in silico* screening to elucidate possible resistant mutation. Molecular docking was employed to screen inhibitors of SARS-CoV-2 from the ZINC ChemDiv database. The top-ranked compounds selected from GOLD docking were further investigated for binding modes at the conserved residues of RdRp, and ten compounds were selected for experimental validation. Of which, three compounds exhibited promising antiviral activity. The most promising candidate showed a half-maximal effective concentration (EC_{50}) of 5.04 μM. Molecular dynamics simulations, binding free-energy calculation and hydrogen bond analysis were performed to elucidate the critical interactions providing a foundation for developing lead compounds effective against SARS-CoV-2.

1. Introduction

The severe acute respiratory syndrome coronavirus 2 (SARS-CoV-2) is a positive-sense, single-stranded RNA virus known to cause the devastating coronavirus disease in 2019 (COVID-19). By December 2021, the infections have reached nearly 266 million global cases and over 5.2 million deaths according to the World Health Organization (WHO). While the available vaccines help mitigate disease severity, vaccinated people may still be infected especially by new variants [1,2]. Moreover, vaccination has not been widely achieved in many countries, thus it alone may not be sufficient to stop the spread. It is most likely now that SARS-CoV-2 might become an endemic virus that continually circulates in the global population [3]. Therefore, there remains a need for development of antiviral therapeutics for people who might be hospitalized with COVID-19.

Coronavirus (CoV) belongs to the Coronaviridae family, which comprises four genera: alpha, beta-, gamma- and delta-coronaviruses, where beta-coronaviruses can be divided into A, B, C, and D lineages [4]. Each CoV genus shares a varying degree of genetics and exhibits wide host adaptability resulting in cross-species transmission [5,6]. In the past two decades, there have been several serious outbreaks of coronaviruses such as severe acute respiratory syndrome (SARS) and human Middle East respiratory syndrome (MERS). SARS-CoV-2 and SARS-CoV belong in the same beta-coronaviruses lineage B while MERS-CoV is in lineage C. Extensive research in MERS-CoV and SARS-CoV in the past have paved the way allowing rapid identification of druggable targets for SARS-CoV-2.

Among the various potential drug targets, viral RNA-dependent RNA polymerase (RdRp) also known as nonstructural protein 12 (nsp12) is considered a promising target. RdRp is indispensable for viral replication [7]. It exhibits conserved core sequences and structural features among RNA viruses, allowing broad antiviral activity design [8]. In SARS-CoV-2, RNA replication required RdRp complex composed of nsp12, nsp7, and nsp8. The nsp12 function

* Corresponding author.
E-mail address: tanaporn.uen@biotec.or.th (T. Uengwetwanit).

https://doi.org/10.1016/j.csbj.2022.02.001

as RdRp is a key component [7] while nsp7 and nsp8 are accessory stimulation of polymerase activity [9]. Remdesivir, the only approved drug by the US Food and Drug Administration for the treatment of COVID-19, is an example of a drug targeting RdRp. Remdesivir has been demonstrated to result in significantly greater recovery for the treatment of COVID-19 in several clinical trials [10-12]. Remdesivir was shown to be most effective when administered in early infection [13,14]. On the other hand, there were studies showing that remdesivir has no statistically significant clinical improvement over the standard-of-care [15-17] especially for patients with severe symptoms and required oxygen support [18]. A combination of remdesivir with other drugs or novel therapeutics such as monoclonal antibodies has been suggested to improve outcomes over Remdesivir alone [19-21].

Here, we report novel inhibitors of SARS-CoV-2 RdRp with promising antiviral activity. Molecular docking was employed to screen inhibitors that showed binding interaction with the conserved residues of RdRp across CoVs. Ten candidate compounds were selected and experimentally validated. Three candidate compounds showed promising antiviral activity with half-maximal effective concentration (EC_{50}) values less than 50 μM. The best promising candidate showed EC_{50} of 5.04 ± 1.11 μM, while EC_{50} of remdesivir was 2.71 ± 0.70 μM. The interactions of the promising compounds and RdRp were investigated by performing molecular dynamics simulations, binding free energy calculations, and hydrogen bond analysis. The knowledge derived from this protein–ligand interaction analysis will be helpful in the further development of effective RdRp inhibitors for coronaviruses.

2. Materials and methods

2.1. Comparative sequence analysis of RdRp CoV

To evaluate conservation of protein binding site among CoVs, RdRp protein sequence of SARS-CoV-2 (Accession ID: QLG75159.1) was used as a query to search RdRp sequence of other CoVs using Blastp against NCBI protein database [22]. The matched sequences were retrieved. Representative sequences of alpha-CoV were HCoV-NL63 (QQY99320.1), HCoV-229E (APD51497.1), Porcine PEDV (ZL47227.1), Bat-CoV/3398–19 (YP_009755889.1), and RH-BAT-CoV-HKU2 (ABQ57215.1). Representative sequences of beta-CoV were divided into three lineages. Lineage A, beta-CoV was presented by HCoV-HKU1 (ABD75591.1), HCoV-OC43 (QXL74882.1), Camel DcCoV-HKU23 (ALA50077.1), and Rabbit RbCoV HKU14. Lineage B, beta-CoV was presented by SARS-CoV (AAP13442.1), SARS-CoV-2 (QLG75159.1), and SARS-CoV-Bat-MA15 (AEA10622.1). Lineage C, beta-CoV was presented by MERS-Cov (QMS54772.1), and Bat HKU5-2 (ABN10883.1). Gamma- and delta-CoV were presented by Dolphin CoV-HKU22 (AHB63507.1) and Bulbul CoV-HKU11-796 (ACJ12043.1), respectively. All protein sequence alignment was re-analyzed using a multiple sequence alignment program (MUSCLE) [23] in UGENE [24]. Percent sequence similarity referred to the percentage of matching sequences between each representative CoV was calculated using MatGAT [25].

2.2. Virtual screening and molecular docking

To discover candidate inhibitors that can bind SARS-CoV-2 RdRp, molecular docking was carried out to screen for potential hit compounds from the Zinc (purchasable ChemDiv library) which contain diverse scaffolds [26]. Multiple compounds' conformations and probable ionized state at pH 7.0 were prepared using Openbabel [27]. The complex structure of the SARS-CoV-2 RdRp and Remdesivir was retrieved from the Protein Data Bank (PDB ID: 7BV2) [28]. Molecular docking was carried out using GOLD (Genetic Optimization for Ligand Docking) with Astex Potential (ASP) scoring function [29]. The binding region was defined by 10 Å from the central of crystalized remdesivir. An option for generating diverse solutions was turned on. The docked protein–ligand complex structures were visualized in Discovery Studio Visualizer Software [30]. Compounds with top ASP scores were purchased from ChemBridge Corporation (San Diego, California) and experimentally tested for their antiviral activity.

2.3. Molecular dynamics (MD) simulation and MM-GBSA assay

Docking pose of hit compounds (compound 2, 8, and 9) in complex with SARS-CoV-2 RdRP and X-ray structure of Remedsivir-SARS-CoV-2 RdRP complex (PDB ID: 7BV2) were subjected to MD simulations. As recently reported, similar protocols and parameters were applied to conduct MD simulations [31]. Briefly, GAFF2 force field together with AM1-BCC charge was utilized to generate essential parameters for ligands, and AMBER ff19SB force field was assigned for protein (SARS-CoV-2 RdRP). The protein–ligand complexes were solvated (10 Å from the molecular surface of the complex) by explicit waters (OPC water model) and counterions (Na^+ or Cl^-). MD simulations were performed using standard conditions (i.e., temperature at 300 K, pressure at 1 bar, time step of 2 fs with SHAKE constraint) and general steps: energy minimization, heating step, followed by equilibration step and finally production run for 50 ns.

Binding free energy (BFE) calculations of protein–ligand complexes were computed by applying the molecular mechanics/generalized Born surface area (MM/GBSA) method using GB model 5 and other related default parameters. One hundred MD snapshots extracted from the last 10 ns (40–50 ns) of MD simulations were exploited for relative BFE calculation by considering only the enthalpy term ($\Delta G_{binding} \sim \Delta H$) and discarding the entropy term ($-T\Delta S$) as previously explained and discussed [31,32]. MD simulations and BFE calculations were conducted by using the AMBER20 program.

2.4. Virus and cells preparation

SARS-CoV-2 can be transmitted through the air, is hazardous to laboratory staff, and requires biological safety levels 3 facility [33]. We, therefore, employed another coronavirus namely porcine epidemic diarrhea virus (PEDV, NCBI accession LC053455) which causes acute diarrhea and dehydration in swine to determine RdRp coronavirus inhibition of hit molecules. PEDV carrying mCherry fluorescent reporter gene (mCherry-PEDV) in its genome was used as a surrogate of coronavirus for antiviral assay. The viral genome was constructed by reverse genetics and the infectious viral particles were prepared as described previously [34]. Vero cells stably expressing eGFP (eGFP-Vero) were established by transfection of the pEGFP-N1 (Clontech) plasmid into Vero cells (ATCC: CCL-81) and selection of the eGFP positive cells using 0.8 mg/ml of G418 antibiotic (Sigma-Aldrich). The cells were maintained in Opti-MEM (Gibgo) supplemented with 10% (v/v) fetal bovine serum and antibiotics.

2.5. Cytotoxicity assay

eGFP-Vero cells were seeded overnight in 96-well tissue culture microplate (at 2.5×10^4 cells/well), at 37 °C in 5% CO_2 incubator. Test compounds and remdesivir were dissolved in dimethyl sulfoxide (DMSO) and added into the cells at the final concentrations of 3.125, 6.25, 12.5, 25, 50, 100, and 200 μM. DMSO-treated cells (0.5% v/v) were used as a control (100% cell viability) for observing cytotoxic effect of the test compounds. After 15 h treatment, cytotoxi-

city was determined by adding Cell Counting Kit-8 reagent (Dojindo) into the cells and incubating the cells for 1 h at 37 °C in 5% CO_2 incubator. Then, the optical density at 450 nm (OD_{450}) was measured by Synergy HTX Multi-Mode Microplate Reader (BioTek) and the percentage of cell viability was calculated by normalization with the DMSO control. Mean values of the normalized cell viability were fit into a dose-respond curve and the half-maximal cytotoxic concentration (CC_{50}) was calculated by GraphPad Prism software.

2.6. Antiviral assay

eGFP-Vero cells were seeded overnight in 96-well CellCarrier Ultra microplate (PerkinElmer) at 2.5×10^4 cells/well at 37 °C in 5% CO_2 incubator. mCherry-PEDV (at the multiplicity of infection of 0.00016) was added into the cells to allow viral absorption (infection) for 1 h at 37 °C. Non-attached viruses were removed by washing the cells with phosphate-buffered saline. Test compounds were dissolved in DMSO and added into the cells with fresh media (Opti-MEM) supplemented with 1% TryPLE (Gibco). DMSO-treated cells (0.5% v/v) were used as a control for observing the antiviral effect of the test compounds. Remdesivir, a viral RNA-dependent RNA polymerase inhibitor that effectively inhibits coronaviruses e.g., SARS-CoV-2 [35] was used as a positive control. At 15 h post-infection, fluorescent images of mCherry (at excitation wavelength 561 nm and emission wavelength 570–630 nm) and eGFP (at excitation wavelength 488 nm and emission wavelength 500–550 nm) were acquired by Opera Phenix high-content screening system (PerkinElmer). The area of mCherry fluorescence (representing syncytia formation from the infection) in each well was specified and the total (or sum) mCherry fluorescent intensity was quantified by Harmony high-content imaging and analysis software (PerkinElmer). The test compounds' relative reduction of mCherry intensity (syncytia formation) was calculated by comparing with the DMSO control. Dose-respond curves were fit using the normalized sum of mCherry fluorescent intensity data and the half-maximal effective concentration (EC_{50}) was calculated by GraphPad Prism software.

3. Results and discussion

3.1. Comparison of RdRp sequences of SARS-CoV-2 with other CoV

Structure of SARS-CoV-2 RdRp contains nidovirus RdRp-associated nucleotidyltransferase (NiRAN) domain, interface domain, and three polymerase domains, namely fingers, palm, and thumb (Fig. 1A) [36]. The polymerase possesses seven conserved motifs, A to G, involved in nucleotide and template binding and catalysis [36]. In this present study, we compared the RdRp protein sequences of four CoV genera and three lineages of beta-coronavirus (Fig. 1B) to explore the possibility of cross binding by inhibitors targeting RdRp. CoV is considered a case of animal-to-human disease transmission. CoV's affecting humans such as SARS-CoV and MERS-CoV, likely originated from bats [37,38]; however, the origin of SARS-CoV-2 is still debated. Apart from highly pathogenic SARS-CoV, MERS-CoV and SARS-CoV-2 that cause human diseases, there are other four human coronaviruses in beta-coronavirus genera including HCoV-NL63, HCoV-229E, HKU1 and HCoV-OC43 that cause mild respiratory tract infection [39]. Protein comparative sequences showed high similarity of RdRp among CoVs. Interestingly, the high sequence similarity of SARS-CoV-2 RdRp ($\geq$75%) was observed among human CoV isolates and animal CoV isolates such as bat, rabbit or porcine (Fig. 1B).

Inspection of sequence similarity of polymerase motifs showed a high identity of SARS-CoV-2 compared with other CoVs (Fig. 1C). Moreover, based on the co-crystallized structure of SARS-CoV-2 RdRp and remdesivir triphosphate (PDB ID: 7BV2) [28], amino acid residues within 4.5 Å of remdesivir triphosphate including Arg553, Arg55, Cys622, Asp623, Ser682, Thr687, Asn691, Ser759, and Asp760 showed high conservation across CoVs. These conserved residues are not part of the mutation profile of RdRp SARS-CoV-2 including non-synonymous variants: P323L and A97V and synonymous variants: Y455Y, N628N, and Y32Y [40-42]. As viruses evolve over the time to adapt and survive in the human host, the emergence of some variants might increase risk to global public health [43]. For example, a recent variant called Omicron (B.1.1.529) poses global concern on effectiveness of current vaccines, tests and treatment [44]. To overcome the effects of possible mutations, we screened inhibitors that not only directly act on RdRp which showed low mutation rate but also bind the conserved residues.

3.2. Virtual screening of candidate SARS-CoV-2 inhibitors

To screen potential SARS-CoV-2 inhibitors, molecular docking was performed using GOLD software, using ASP scoring function. Compounds from the purchasable Zinc ChemDiv library were docked into the binding pocket of the SARS-CoV-2 RdRp structure to predict the binding affinity. The compounds with top-ranked docking results were further investigated for their binding mode. As hydrogen bonds are imperative to binding affinity and specific interaction, the candidate compounds should have at least one hydrogen bond interaction with the conserved catalytic active residues as aforementioned. Finally, the top ten hits were selected as the final candidates. The 2D structures, docking scores, and detail of physiochemical properties of the selected candidates are depicted in Fig. 2. The drug-like criteria as Lipinski's rule of five including molecular mass less than 500 Da, less than 5 hydrogen bond donors, less than 10 hydrogen bond acceptors and an octanol–water partition coefficient log P less than 5, were investigated [45]. The results showed that the candidate compounds have no more than one violation of the drug-like criteria. Only compound 9 has slightly higher molecular weight (571 Da) than the criteria of 500 Da, nevertheless its weight was not higher than the average molecular mass of orally available FDA-approved drugs (600 Da) [46].

3.3. Antiviral activity and cytotoxicity

To evaluate antiviral activity of the hit compounds derived from *in silico* screening against coronavirus, PEDV, a non-zoonotic virus belonging to the alpha-coronavirus genus was used as a surrogate for antiviral assay. In this study, we used the PEDV model to test potential inhibitors of SARS-CoV-2 because PEDV is not a risk to human health [47] and permissible for experiment in our laboratory. Furthermore, protein sequences of coronaviruses' polymerase are conserved, and the candidates were designed based on those conserved amino acids. The potential inhibitors, therefore, are expected to inhibit coronaviruses. Remdesivir, the only FDA-approved drug for COVID-19, was used as a positive control because it showed antiviral activity against RdRp of various RNA viruses such as Ebola virus, MERS virus, SARS-CoV [48-50] as well as PEDV [51]. Previously, the concept of using the PEDV model to test potential inhibitors of SARS-CoV-2 has been performed to evaluate a SARS-CoV-2 protease inhibitor which is a highly conserved protein among coronaviruses [52].

Vero cells stably expressing eGFP were used as a host cell for infection with the reporter PEDV carrying mCherry fluorescent gene (mCherry-PEDV) of which the expression of reporter protein occurred only after transcription and replication processes of virus

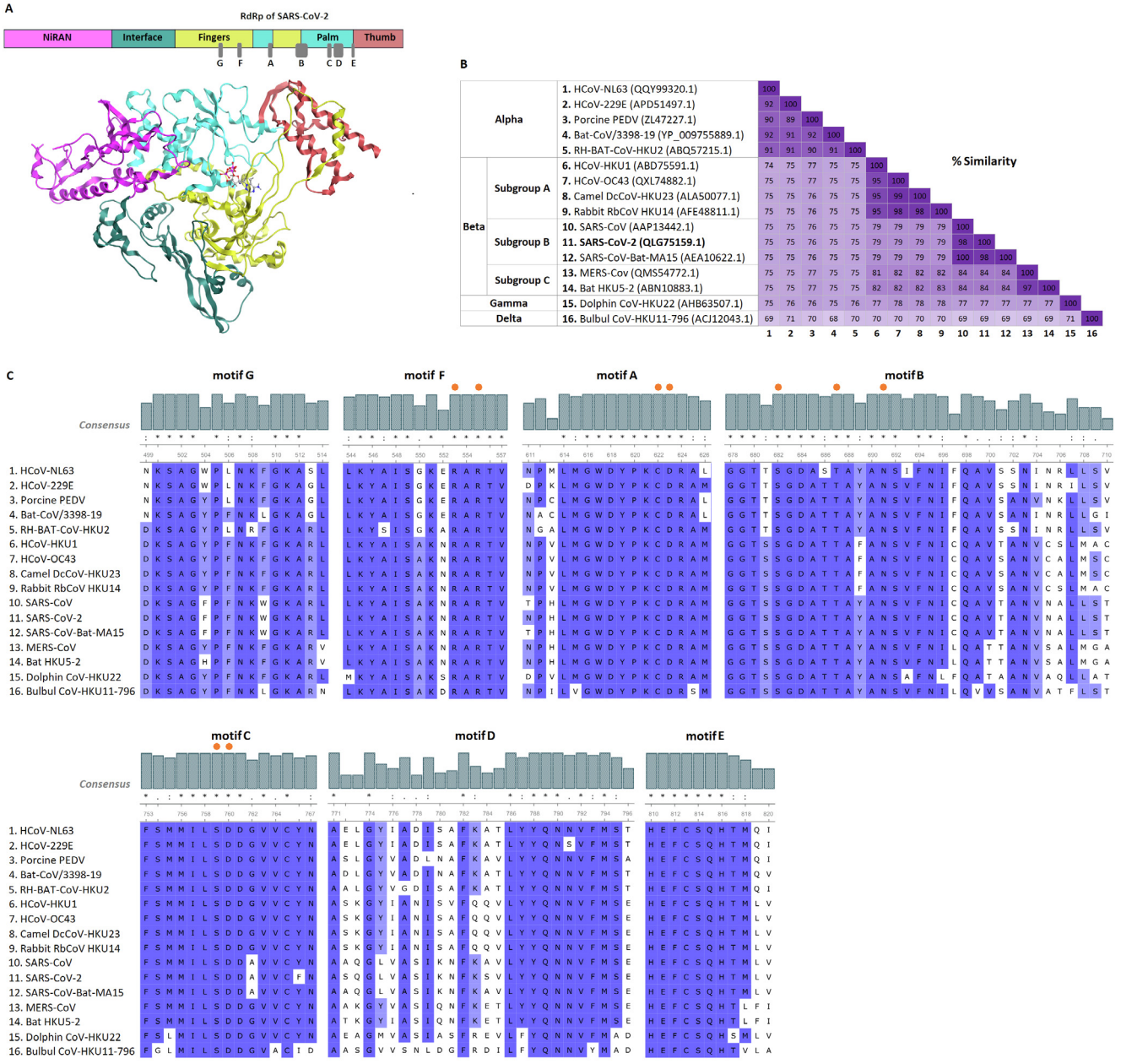

Fig. 1. SARS-CoV-2 RNA-dependent RNA polymerase (RdRp). (A) Schematic diagram of domain organization of the SARS-CoV-2 RdRp and its structure. (B) Matrix of percentage protein sequence similarity values calculated from pairwise alignment of 16 coronavirus RdRp representing alpha-, beta-, gamma- and delta-coronaviruses. (C) Multiple sequence aligment of seven conserved motifs (A, B, C, D, E, F and G) of SARS-CoV-2 RdRp compared to other RdRp coronaviruses. Identical residues are shown in blue. Top bars indicate the percentage of consensus sequences at each residue. Orange dots above the bars indicate the residues within 4.5 Å of Remdesivir triphosphate. (For interpretation of the references to colour in this figure legend, the reader is referred to the web version of this article.)

in host cells [34]. Therefore, the cytopathic effect of infected cells was observed by the formation of syncytia with mCherry protein (Fig. 3). Most hit compounds have no cytotoxicity at the concentration of 100 μM whereas compound 2 was toxic to the cells at CC_{50} values of 26.58 ± 6.84 μM (Fig. S1 and Table S1). Non-cytotoxic concentrations of the hit compounds were used for further antiviral assay.

Treating the infected cells with remdesivir (50 μM), an inhibitor of viral RdRp which effectively inhibits replication of other coronaviruses such as SARS-CoV-2 [35], completely inhibited mCherry expression and syncytia formation (Fig. 3) indicating that this replication system is suitable for antiviral assay. Effective inhibition of viral replication was also observed when treating the infected cells with compound 2 at 15 μM (Fig. 3). In addition, compound 8 and 9 showed a partial antiviral effect against viral replication at the concentration of 50 μM (Fig. 3). Compound 2, 8, and 9 were selected for further antiviral assay with various concentrations of the compounds for dose–response curve fitting and estimation of EC_{50} value. Treating the infected cells with test compounds or remdesivir (a positive control) reduced viral replication in a dose-dependent manner (Fig. S2). Estimating EC_{50} values from the dose–response curves showed that compound 2 inhibited viral replications at EC_{50} of 5.04 ± 1.11 μM with the selectivity index (SI) value of 5 (Fig. S2 and Table 1). Compound 8 and 9 inhibited viruses at EC_{50} of 29.32 ± 4.91 μM (SI > 3) and 51.14 ± 5.45 μM (SI > 2), respectively, whereas remdesivir inhibited virus at EC_{50} of

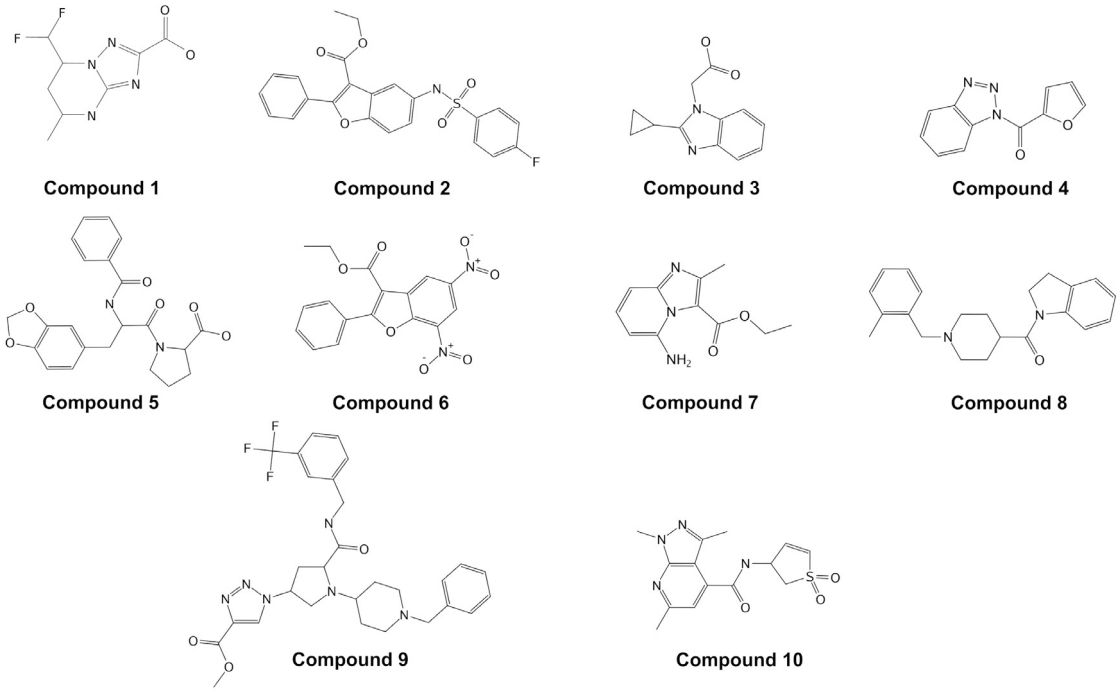

	Compound	ASP score	MW (Da)	LogP	H-bond donor count	H-bond acceptor count
1.	7-(difluoromethyl)-5-methyl-4,5,6,7-tetrahydro [1,2,4] triazolo[1,5-a] pyrimidine-2-carboxylic acid	60.63	232	1.89	2	4
2.	Ethyl 5-[[(4-fluorophenyl) sulfonyl] amino}-2-phenyl-1-benzofuran-3-carboxylate	64.83	439	6.27	1	5
3.	(2-cyclopropyl-1H-benzimidazol-1-yl) acetic acid	63.67	216	1.68	1	3
4.	1-(2-furoyl)-1H-1,2,3-benzotriazole	57.09	213	3.39	0	5
5.	3-(1,3-benzodioxol-5-yl)-N-benzoylalanylproline	61.36	410	2.29	2	6
6.	Ethyl 5,7-dinitro-2-phenyl-1-benzofuran-3-carboxylate	66.48	356	3.88	0	7
7.	Ethyl 5-amino-2-methylimidazo[1,2-a] pyridine-3-carboxylate	52.66	219	1.55	1	3
8.	1-[[1-(2-methylbenzyl)-4-piperidinyl] carbonyl] indoline	59.11	334	3.66	0	2
9.	Methyl 1-[(3S,5S)-1-(1-benzyl-4-piperidinyl)-5-([[3-(trifluoromethyl) benzyl] amino] carbonyl)-3-pyrrolidinyl]-1H-1,2,3-triazole-4-carboxylate	65.02	571	4.78	1	8
10.	10. N-(1,1-dioxido-2,3-dihydro-3-thienyl)-1,3,6-trimethyl-1H-pyrazolo[3,4-b] pyridine-4-carboxamide	58.24	320	-0.43	1	5

Fig. 2. Structures and physicochemical properties of the ten selected compounds.

2.71 ± 0.70 μM (SI > 37) (Fig. S2 and Table 1). These results verify that *in silico* targeting RdRp with the compound 2, 8, or 9 effectively inhibited *in vitro* replication of coronavirus.

3.4. Molecular dynamic simulation and MM-GBSA

The antiviral assay revealed that the three selected compounds showed promising antiviral activity. The protein–ligand complexes were subjected to MD simulations to gain insight into the atomic interactions of these hit compounds with SARS-CoV-2 RdRp. Remdesivir is a nucleotide analog prodrug that is metabolized into an active form, remdesivir triphosphate (RTP) recognized by viral RdRp [28]. RTP then competes with ATP for incorporation into the growing viral RNA chain and causes RNA synthesis arrest [28]. RTP, therefore, was used to study binding interaction and binding free energy. The promising candidates which are not nucleotide analogs were targeted to bind the same pocket as RTP. Binding interactions of the candidates and RTP with SARS-CoV-2 RdRp were investigated to guide interactions that might improve inhibitory activity in further study. The stability of the protein–ligand complex was evaluated through root-mean-square deviation (RMSD), which is the difference between the backbones of the protein from its initial structure to its final position (Fig. S3). It could be observed that the complex structures of

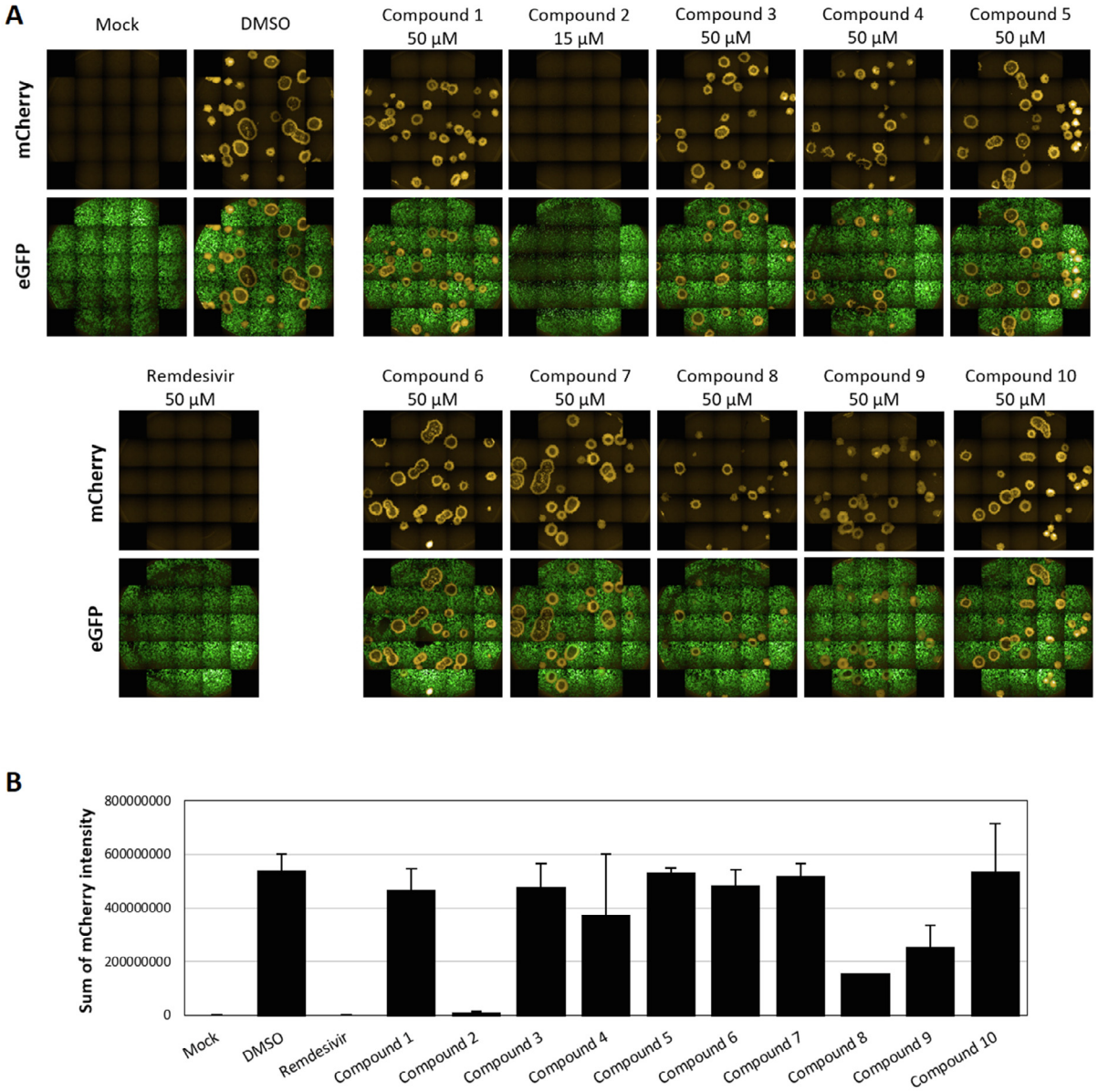

Fig. 3. Anti-coronavirus effect of test compounds. (A) eGFP-Vero cells in 96-well plate were infected with mCherry-PEDV and treated with compound 1, 2, 3, 4, 5, 6, 7, 8, 9, 10, or Remdesivir (as a positive control) at the indicated concentrations. DMSO treated cells were used as the control for observing the inhibitory effect of the test compounds. Mock is the DMSO-treated cells without virus infection. At 15 h post-infection, images of mCherry and eGFP fluorescent signals at 21 images/well, were acquired by Opera Phenix high-content screening system. (B) The sum of mCherry fluorescent intensity in each well of A was quantified by Harmony software and the mean values (±SD) from two independent experiments (each performed in duplicate) are shown.

Table 1
Half-maximal effective concentration (EC_{50}) and selectivity index (SI) of compound 2, 8, and 9.

Compound	EC_{50} ± SD (μM)	SI (=CC_{50}/EC_{50})
2	5.04 ± 1.11	5
8	29.32 ± 4.91	>3
9	51.14 ± 5.45	>2
Remdesivir	2.71 ± 0.70	>37

the candidate compounds displayed slight fluctuation over 50-ns simulation as observed in the co-crystallized remdesivir structure. The simulation results showed that all systems had converged well, and these candidates formed stable bindings with the target protein. The MM-GBSA based binding free energy of remdesivir triphosphate, compound 2, compound 8 and compound 9 in the complex were −184.36 ± 11.27 kcal/mol (-771.36 ± 47.15 kJ/mol), −37.35 ± 3.92 kcal/mol (-156.27 ± 13.77 kJ/mol), −32.67 ± 3.62 kcal/mol (-136.69 ± 15.15 kJ/mol) and −26.29 ± 5.55 kcal/mol (-110.00 ± 23.22 kJ/mol), respectively (Fig. 4). The negative binding free energy of the compounds agreed with the experimental ranking antiviral activity Fig. S3.

3.5. Analysis of binding poses of the promising candidates

As key molecular interactions formed between potential candidates and protein target are essential to guide structure–activity optimization, binding interaction of promising antiviral candidates was analyzed. The binding interaction of remdesivir triphosphate exhibited several attractive charge interactions between triphosphate and the residues Arg553, Arg555 and divalent magnesium (Fig. 4A) as previously reported [53,54]. Analysis of traditional

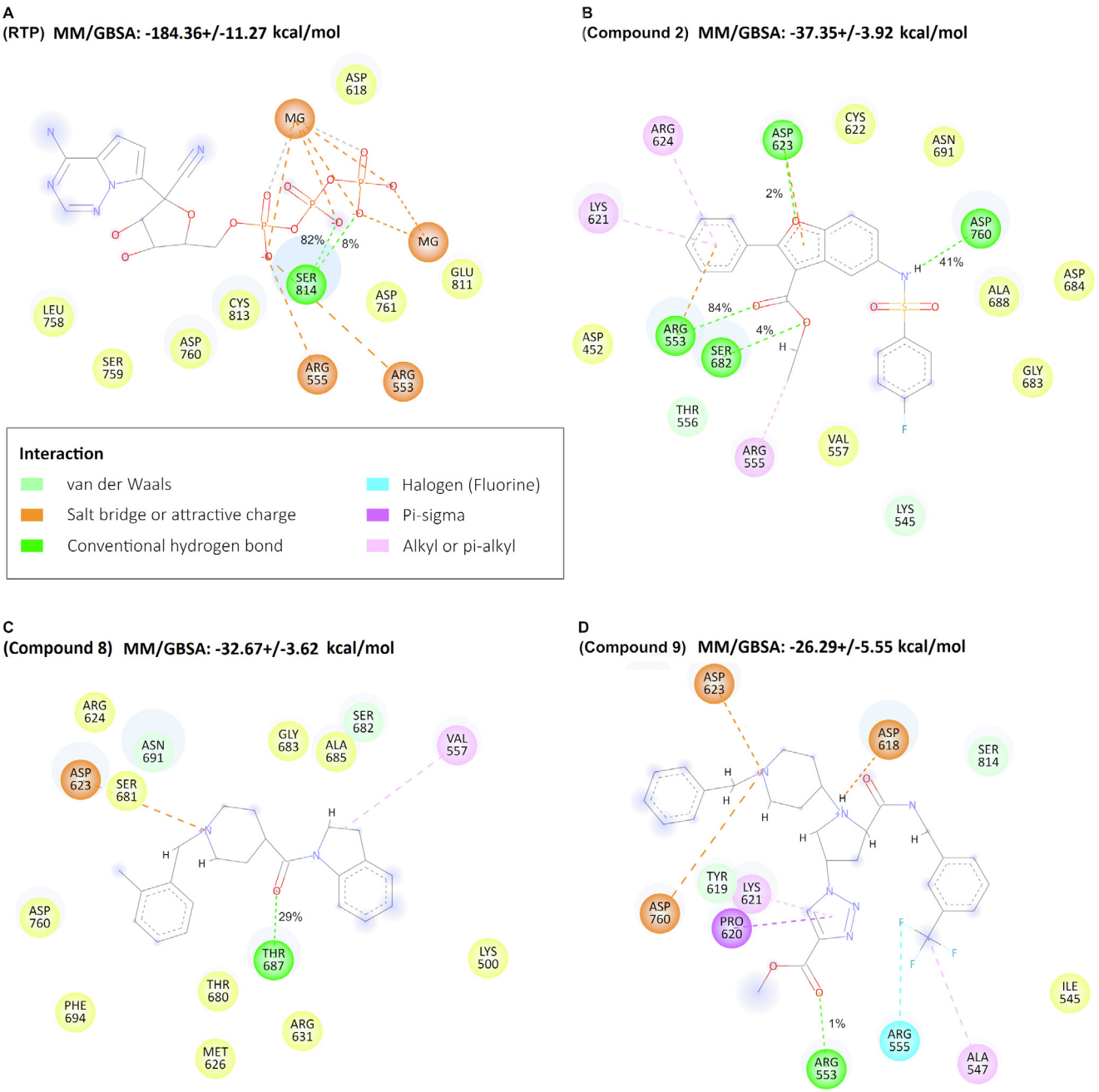

Fig. 4. 2D ligand interaction diagrams of the inhibitors into the catalytic binding site of RNA-dependent-RNA-polymerase (RdRp) SARS-CoV-2 (Discovery Studio Client version 2021). The inhibitors are (A) Remdesivir triphosphate (RTP), (B) Compound 2 (C) Compound 8 and (D) Compound 9. The binding free energy and energy components (kcal/mol) for the protein-inhibitor complexes predicted by the MM/GBSA method. The percentage occupancy of H-bonds averaged over the last 50 ns of simulation time was present along the green dashed lines. (For interpretation of the references to colour in this figure legend, the reader is referred to the web version of this article.)

hydrogen bond occupancy, which is the angle and the distance between the donors and the acceptors are less than 135°Å and 3.0 Å (acceptor to donor heavy atom), respectively, showed 82% hydrogen bond occupancy between Ser814 phosphate group (Fig. 4B). Compared to our candidate compounds, the interaction of compound 2, 8 and 9 showed different binding modes. Compound 2 which exhibited the highest binding affinity among the candidate compounds, showed high hydrogen bond occupancy as remdesivir. Two hydrogen bonds of compound 2 were interaction between the carboxylate oxygen atom and Arg553 (82% hydrogen occupancy) and the oxygen atom of the benzofuran ring and Asp760 (41% hydrogen bond occupancy). Both Arg553 and Asp760 are conserved amino acid residues in RdRp of CoVs. Apart from the hydrogen bond interaction, Pi-alkyl hydrophobic interactions were observed with Arg624 and Lys621.

Weaker anti-CoVs of compound 8 and 9 showed much lower hydrogen bond occupancy than compound 2 (Fig. 4C and Fig. 4D). Compound 8 showed 29% hydrogen bond occupancy between carbonyl and Thr687 while compound 9 exhibited no significant hydrogen bonding. The primary affinity of compound 9 was attractive interaction between N of 4-pyrrolidinyl with Asp623 and Asp760, and Pi-sigma /Pi-alkyl between triazole and Lys621 and Pro620. It suggested that hydrophobic interactions could improve the binding in further studies.

The results reported herein should be considered with some limitations. First, the PEDV model was employed to screen antiviral activity. This model might be useful for screening coronavirus antiviral agents. Nonetheless, the quantitative antiviral activity found in the PEDV model might be different from inhibition activity in SARS-CoV-2. Although it has been reported that remdesivir's antiviral activity is variable in different cell types [55], the ranking of the compounds based on binding free energy prediction in SARS-CoV-2 polymerase was similar to the result obtained from antiviral activity assay in PEDV. Antiviral activity test on SARS-CoV-2, therefore, is necessary to quantitative antiviral potency for further structure/activity relationship analysis. The second limitation concerns the cell line. The Vero cell line employed in this study is derived from a monkey kidney whereas lung epithelial cells are regarded to be the main targets for SARS-CoV-2 infection in humans [56]. Drug metabolism or bioavailability may not be represented in Vero cells.

4. Conclusions

In an attempt to identify novel candidate compounds to fight against SARS-CoV-2, we have selected RpRd as a potential drug target. We analyzed RpRd protein sequences to ensure high sequence conservation across coronaviruses and to evaluate its feasibility as a target for combating emerging CoV outbreaks. While most *in silico* screening used the conserved interactions between remdesivir and residues of RdRp for identified novel inhibitors, we employed an alternative approach by utilizing molecular docking to screen compounds and curate the binding interaction based on the conserved residues of RdRp. Three potential inhibitors (compound 2, 8 and 9) have been experimentally validated. Although inhibition activity was not directly evaluated on SARS-CoV-2 but on another coronavirus (PEDV) instead, the promising results showed the inhibitors might be broadly effective. The MD simulations revealed key interactions. The information of these active inhibitors provides a novel guide for inhibitor design which will enable us to develop a competent drug that might be complementary in treatment or reduce the likelihood of resistance. Further validation on SARS-CoV-2 and mutants will be required on the path toward developing SARS-CoV-2 inhibitors.

Declaration of Competing Interest

The authors declare that they have no known competing financial interests or personal relationships that could have appeared to influence the work reported in this paper.

Acknowledgments

This work was financially supported by the grant from the National Center for Genetic Engineering and Biotechnology (BIOTEC), Thailand (Grant No. P-2051635). We appreciate Dr. Anan Jongkaewwattana and Dr. Vanicha Vichai (National Center for Genetic Engineering and Biotechnology) for providing mCherry-PEDV and eGFP-Vero cells, respectively, for experimental validation.

Appendix A. Supplementary data

Supplementary data to this article can be found online at https://doi.org/10.1016/j.csbj.2022.02.001.

References

[1] Lopez Bernal J, Andrews N, Gower C, Gallagher E, Simmons R, Thelwall S, et al. Effectiveness of Covid-19 Vaccines against the B.1.617.2 (Delta) Variant. N Engl J Med 2021;385(7):585–94.
[2] Puranik A, Lenehan PJ, Silvert E, Niesen MJM, Corchado-Garcia J, O'Horo JC, et al. **Comparison of two highly-effective mRNA vaccines for COVID-19 during periods of Alpha and Delta variant prevalence**. medRxiv 2021. https://doi.org/10.1101/2021.08.06.21261707.
[3] Phillips N. The coronavirus is here to stay - here's what that means. Nature 2021;590(7846):382–4.
[4] Woo PCY, Lau SKP, Lam CSF, Lau CCY, Tsang AKL, Lau JHN, et al. Discovery of seven novel Mammalian and avian coronaviruses in the genus deltacoronavirus supports bat coronaviruses as the gene source of alphacoronavirus and betacoronavirus and avian coronaviruses as the gene source of gammacoronavirus and deltacoronavirus. J Virol 2012;86(7):3995–4008.
[5] Shi Z. From SARS, MERS to COVID-19: A journey to understand bat coronaviruses. Bull Acad Natl Med 2021;205(7):732–6.
[6] Dhama K, Patel SK, Sharun K, Pathak M, Tiwari R, Yatoo MI, et al. SARS-CoV-2 jumping the species barrier: Zoonotic lessons from SARS, MERS and recent advances to combat this pandemic virus. Travel Med Infect Dis 2020;37:101830.
[7] Ahn D-G, Choi J-K, Taylor DR, Oh J-W. Biochemical characterization of a recombinant SARS coronavirus nsp12 RNA-dependent RNA polymerase capable of copying viral RNA templates. Arch Virol 2012;157(11):2095–104.
[8] de Farias ST, dos Santos Junior AP, Rêgo TG, José MV. Origin and Evolution of RNA-Dependent RNA Polymerase. Front Genet 2017;8:125.
[9] Hillen HS, Kokic G, Farnung L, Dienemann C, Tegunov D, Cramer P. Structure of replicating SARS-CoV-2 polymerase. Nature 2020;584(7819):154–6.
[10] Beigel JH, Tomashek KM, Dodd LE, Mehta AK, Zingman BS, Kalil AC, et al. Remdesivir for the Treatment of Covid-19 — Final Report. N Engl J Med 2020;383(19):1813–26.
[11] Olender SA, Perez KK, Go AS, Balani B, Price-Haywood EG, Shah NS, et al. Remdesivir for Severe Coronavirus Disease 2019 (COVID-19) Versus a Cohort Receiving Standard of Care. Clin Infect Dis 2021;73(11):e4166–74.
[12] Al-Abdouh A, Bizanti A, Barbarawi M, Jabri A, Kumar A, Fashanu O, et al. Remdesivir for the treatment of COVID-19: A systematic review and meta-analysis of randomized controlled trials. Contemp Clin Trials 2021;101:106272.
[13] Dölken L, Stich A, Spinner CD. Remdesivir for Early COVID-19 treatment of high-risk individuals prior to or at early disease onset-lessons learned. Viruses 2021;13(6):963.
[14] Gottlieb RL, Vaca CE, Paredes R, Mera J, Webb BJ, Perez G, et al. Early remdesivir to prevent progression to severe covid-19 in outpatients. N Engl J Med 2021;386(4):305–15.
[15] Mahajan L, Singh AP, Gifty. Clinical outcomes of using remdesivir in patients with moderate to severe COVID-19: A prospective randomised study. Indian J Anaesthesia 2021;65(Suppl 1).
[16] Russo A, Binetti E, Borrazzo C, Cacciola EG, Battistini L, Ceccarelli G, et al. *Efficacy of Remdesivir-Containing Therapy in Hospitalized COVID-19 Patients: A Prospective Clinical Experience*. Journal of. Clinical Medicine 2021;10(17):3784.
[17] Yan VC, Muller FL. Why remdesivir failed: preclinical assumptions overestimate the clinical efficacy of remdesivir for COVID-19 and ebola. Antimicrob Agents Chemother 2021;65(10).
[18] Ader F, Bouscambert-Duchamp M, Hites M, Peiffer-Smadja N, Poissy J, Belhadi D, et al. Remdesivir plus standard of care versus standard of care alone for the treatment of patients admitted to hospital with COVID-19 (DisCoVeRy): a phase 3, randomised, controlled, open-label trial. Lancet Infect Dis 2021;22(2):209–21.
[19] Sun D. Remdesivir for Treatment of COVID-19: Combination of Pulmonary and IV Administration May Offer Aditional Benefit. Aaps j 2020;22(4):77.
[20] Martinez DR, Schäfer A, Leist SR, Li D, Gully K, Yount B, et al. Prevention and therapy of SARS-CoV-2 and the B.1.351 variant in mice. Cell reports 2021;36(4):109450.
[21] Taha HR, Keewan N, Slati F, Al-Sawalha NA. Remdesivir: A closer look at its effect in COVID-19 pandemic. Pharmacology 2021;106(9-10):462–8.
[22] Camacho C, Coulouris G, Avagyan V, Ma N, Papadopoulos J, Bealer K, et al. BLAST+: architecture and applications. BMC Bioinf 2009;10:421.
[23] Edgar RC. MUSCLE: a multiple sequence alignment method with reduced time and space complexity. BMC Bioinf 2004;5(1):113.
[24] Okonechnikov K, Golosova O, Fursov M. Unipro UGENE: a unified bioinformatics toolkit. Bioinformatics 2012;28(8):1166–7.
[25] Campanella JJ, Bitincka L, Smalley J. MatGAT: An application that generates similarity/identity matrices using protein or DNA sequences. BMC Bioinf 2003;4(1):29.
[26] Irwin JJ, Tang KG, Young J, Dandarchuluun C, Wong BR, Khurelbaatar M, et al. ZINC20-A free ultralarge-scale chemical database for ligand discovery. J Chem Inf Model 2020;60(12):6065–73.
[27] O'Boyle NM, Banck M, James CA, Morley C, Vandermeersch T, Hutchison GR. Open Babel: An open chemical toolbox. J Cheminf 2011;3(1).
[28] Yin W, Mao C, Luan X, Shen D-D, Shen Q, Su H, et al. Structural basis for inhibition of the RNA-dependent RNA polymerase from SARS-CoV-2 by remdesivir. Science 2020;368(6498):1499–504.

[29] Verdonk ML, Cole JC, Hartshorn MJ, Murray CW, Taylor RD. Improved protein-ligand docking using GOLD. Proteins 2003;52(4):609–23.
[30] Dassault Systemes BIOVIA, BIOVIA Discovery Studio Visualizer v.4.0. 2021, San Diego: Dassault Systemes, 2021. Available from: https://discover.3ds.com/discovery-studio-visualizer-download
[31] Wichapong K, Silvestre-Roig C, Braster Q, Schumski A, Soehnlein O, Nicolaes GAF. Structure-based peptide design targeting intrinsically disordered proteins: Novel histone H4 and H2A peptidic inhibitors. Comput Struct Biotechnol J 2021;19:934–48.
[32] Wichapong K, Alard J-E, Ortega-Gomez A, Weber C, Hackeng TM, Soehnlein O, et al. Structure-Based Design of Peptidic Inhibitors of the Interaction between CC Chemokine Ligand 5 (CCL5) and Human Neutrophil Peptides 1 (HNP1). J Med Chem 2016;59(9):4289–301.
[33] Kaufer AM, Theis T, Lau KA, Gray JL, Rawlinson WD. Laboratory biosafety measures involving SARS-CoV-2 and the classification as a Risk Group 3 biological agent. Pathology 2020;52(7):790–5.
[34] Jengarn J, Wongthida P, Wanasen N, Frantz PN, Wanitchang A, Jongkaewwattana A. Genetic manipulation of porcine epidemic diarrhoea virus recovered from a full-length infectious cDNA clone. J Gen Virol 2015;96(8):2206–18.
[35] Wang M, Cao R, Zhang L, Yang X, Liu J, Xu M, et al. Remdesivir and chloroquine effectively inhibit the recently emerged novel coronavirus (2019-nCoV) in vitro. Cell Res 2020;30(3):269–71.
[36] Kirchdoerfer RN, Ward AB. Structure of the SARS-CoV nsp12 polymerase bound to nsp7 and nsp8 co-factors. Nat Commun 2019;10(1):2342.
[37] Forni D, Cagliani R, Clerici M, Sironi M. Molecular evolution of human coronavirus genomes. Trends Microbiol 2017;25(1):35–48.
[38] Tao Y, Shi M, Chommanard C, Queen K, Zhang J, Markotter W, et al. Surveillance of bat coronaviruses in Kenya identifies relatives of human coronaviruses NL63 and 229E and their recombination history. J Virol 2017;91(5).
[39] Liu DX, Liang JQ, Fung TS. Human coronavirus-229E, -OC43, -NL63, and -HKU1 (Coronaviridae). Encyclop Virol 2021:428–40.
[40] Ilmjärv S, Abdul F, Acosta-Gutiérrez S, Estarellas C, Galdadas I, Casimir M, et al. Concurrent mutations in RNA-dependent RNA polymerase and spike protein emerged as the epidemiologically most successful SARS-CoV-2 variant. Sci Rep 2021;11(1).
[41] Eskier D, Karakülah G, Suner A, Oktay Y. RdRp mutations are associated with SARS-CoV-2 genome evolution. PeerJ 2020;8:e9587.
[42] Wang R, Hozumi Y, Yin C, Wei G-W. Decoding SARS-CoV-2 transmission and evolution and ramifications for COVID-19 diagnosis, vaccine, and medicine. J Chem Inf Model 2020;60(12):5853–65.
[43] World Health Organization. *Tracking SARS-CoV-2 variants*. 2021 [cited 2021 November 26]; Available from: https://www.who.int/en/activities/tracking-SARS-CoV-2-variants/.
[44] World Health Organization. *Classification of Omicron (B.1.1.529): SARS-CoV-2 Variant of Concern*. 2021 [cited 2021 26 November]; Available from: https://www.who.int/news/item/26-11-2021-classification-of-omicron-(b.1.1.529)-sars-cov-2-variant-of-concern.
[45] Lipinski CA. Lead- and drug-like compounds: the rule-of-five revolution. Drug Discov Today Technol 2004;1(4):337–41.
[46] Mullard A. Re-assessing the rule of 5, two decades on. Nat Rev Drug Discov 2018;17(11):777.
[47] Jung K, Saif LJ, Wang Q. Porcine epidemic diarrhea virus (PEDV): An update on etiology, transmission, pathogenesis, and prevention and control. Virus Res 2020;286:198045.
[48] Sheahan TP, Sims AC, Graham RL, Menachery VD, Gralinski LE, Case JB, et al. Broad-spectrum antiviral GS-5734 inhibits both epidemic and zoonotic coronaviruses. Sci Transl Med 2017;9(396).
[49] Santoro MG, Carafoli E. Remdesivir: From Ebola to COVID-19. Biochem Biophys Res Commun 2021;538:145–50.
[50] Brown AJ, Won JJ, Graham RL, Dinnon KH, Sims AC, Feng JY, et al. Broad spectrum antiviral remdesivir inhibits human endemic and zoonotic deltacoronaviruses with a highly divergent RNA dependent RNA polymerase. Antiviral Res 2019;169:104541.
[51] Xie Y, Guo X, Hu T, Wei D, Ma X, Wu J, et al. Significant inhibition of porcine epidemic diarrhea virus in vitro by remdesivir, its parent nucleoside and β-d-N4-hydroxycytidine. Virol Sin 2021;36(5):997–1005.
[52] Lin Y, Zang R, Ma Y, Wang Z, Li Li, Ding S, et al. Xanthohumol is a potent pan-inhibitor of coronaviruses targeting main protease. Int J Mol Sci 2021;22(22):12134.
[53] Long C, Romero ME, La Rocco D, Yu J. Dissecting nucleotide selectivity in viral RNA polymerases. Comput Struct Biotechnol J 2021;19:3339–48.
[54] Koulgi S, Jani V, Uppuladinne MVN, Sonavane U, Joshi R. Remdesivir-bound and ligand-free simulations reveal the probable mechanism of inhibiting the RNA dependent RNA polymerase of severe acute respiratory syndrome coronavirus 2. RSC Adv 2020;10(45):26792–803.
[55] Yan V, Florian M. Comprehensive Summary Supporting Clinical Investigation of GS-441524 for Covid-19 Treatment. OSF Preprints. 2020. https://doi.org/10.31219/osf.io/mnhxu.
[56] Essaidi-Laziosi M, Javier Perez Rodriguez F, Hulo N, Jacquerioz F, Kaiser L, Eckerle I. Estimating clinical SARS-CoV-2 infectiousness in Vero E6 and primary airway epithelial cells. Lancet Microbe 2021;2(11).